A&A 450, 407–413 (2006)
DOI: 10.1051/0004-6361:20054474

Astronomy & Astrophysics

Improved oscillator strengths and wavelengths in Hf II, with applications to stellar elemental abundances⋆

M. Lundqvist[1], H. Nilsson[1], G. M. Wahlgren[1], H. Lundberg[2], H. L. Xu[2,3,4], Z.-K. Jang[3], and D. S. Leckrone[5]

[1] Atomic Astrophysics, Lund Observatory, Lund University, Box 43, 221 00 Lund, Sweden
e-mail: martin.lundqvist@astro.lu.se
[2] Atomic Physics, Department of Physics, Lund Institute of Technology, Box 118, 221 00 Lund, Sweden
[3] Department of Physics, Jilin University, ChangChun, 130023, PR China
[4] Department of Physics, Engineering and Optics, Laval University, Quebec City, G1K 7P4, Canada
[5] Laboratory for Astronomy and Solar Physics, NASA Goddard Space Flight Center, Code 681, Greenbelt, MD, 20771, USA

Received 4 November 2005 / Accepted 29 December 2005

ABSTRACT

Aims. We present new and improved radiative lifetimes for eight levels in Hf I and 18 levels in Hf II, along with oscillator strengths and wavelengths for 195 transitions in Hf II. With these data we determine the abundance of hafnium in two chemically peculiar stars: the hot-Am star HR 3383 and the HgMn star χ Lupi, and discuss the implications of the new data to the hafnium abundance for the Sun and the metal-poor galactic halo stars CS 22892-052 and CS 31082-001.

Methods. The oscillator strengths are derived by combining radiative lifetimes measured with the laser induced fluorescence technique and branching fractions determined from intensity calibrated Fourier transform spectra. The hafnium abundance in the two sharp-lined peculair stars is determined by comparison of spectra obtained from instruments onboard the *Hubble Space Telescope* with synthetic spectra, while the abundance of hafnium in the solar photosphere and the metal-poor halo stars is discussed in terms of rescaling previous investigations using the new gf values.

Results. The abundance enhancement of hafnium has been determined in HR 3383 to be +1.7 dex and that for χ Lupi A is +1.3 dex. In the course of the analysis we have also determined an abundance enhancement for molybdenum in HR 3383 to be +1.2 dex, which is similar to that known for χ Lupi A. The abundances in the metal-poor halo stars CS 31082-001 and CS 22892-052 were rescaled to $\log \epsilon(\mathrm{Hf}) = -0.75$ and −0.82 respectively, with smaller 1σ uncertainty. This has the effect of improving the theoretical fits of r-process nucleosynthesis to abundance data for heavy elements. The change of gf values also implies that the hafnium abundance in the solar photosphere should be reduced by up to 0.2 dex, thereby inducing a discrepancy with the meteoritic hafnium abundance.

Key words. atomic data – line: identification – stars: abundances

1. Introduction

Hafnium is a heavy trace element ($Z = 72$) that has been investigated in relatively few stars. However, it can be an element of interest to diverse fields, such as elemental diffusion in the atmospheres of chemically peculiar (CP) stars and chemical evolution from old galactic halo stars, by virtue of its numerous stable isotopes.

The solar photospheric abundance of hafnium, $\log \epsilon(\mathrm{Hf}) = 0.88 \pm 0.08$, on a scale where $\log \epsilon(\mathrm{H}) = 12.00$, is currently attributed to the work of Andersen et al. (1976), who determined this abundance from synthetic spectrum fitting of six lines in the solar spectrum. At this abundance level, hafnium is among the least abundant elements in nature. Other examples of hafnium abundance determination include the solar-like abundance for the bright F0 Ib star Canopus (Reynolds et al. 1988), the work of Yushchenko et al. (2005b) for δ Scuti in determining an abundance pattern similar to that for Am-Fm stars, and the enigmatic roAp star HD 101065 (Cowley et al. 2000).

Sneden et al. (1996) claimed a first detection of Hf II in a metal-poor halo star. They detected two Hf II lines ($\lambda\lambda$3719.28, 3793.38 Å) in the spectrum of CS 22892-052, with a mean abundance of $\log \epsilon = -0.90 \pm 0.10$ (1σ uncertainty 0.14). They compared their results for a number of heavy elements to calculations of the contribution of r- and s-processes in the solar abundances, scaling the solar pattern to best match the abundances of the elements $56 \leq Z \leq 76$. This gave clear indications of a pure r-process contribution to the heavy element abundances of CS 22982-052. Later, Sneden et al. (2003) reanalyzed the elemental abundances in CS 22892-052 resulting in a mean hafnium abundance of $\log \epsilon = -0.98 \pm 0.10$.

⋆ Tables 3–6 are only available in electronic form at http://www.edpsciences.org

Hill et al. (2002) derived abundances for a large number of elements in the metal-poor halo star CS 31082-001. The use of two Hf II lines ($\lambda\lambda$3399.793, 3719.276) lead to an abundance of $\log \epsilon = -0.59 \pm 0.21$. Abundances were compared with a calculated scaled solar *r*-process pattern, resulting in a good fit to the abundances of the elements between barium and thulium. However, the fit for several elements, including hafnium, osmium and lead, fell outside the assignment of the uncertainties. In the case of osmium the discrepancy would later be ascribed to the atomic data, and with new gf values (Ivarsson et al. 2003) the osmium abundance also fit the solar *r*-process pattern.

Yushchenko et al. (2005a) investigated the Hf II λ4093.155 line in the halo star HD 221170, deriving a hafnium enhancement relative to iron that places it above the scaled *r*-process abundance distribution for heavy elements. Based on their work with a number of heavy elements they conclude that the *r*-process is not universal.

The Hf II line data used to interpret stellar spectra dates back more than forty years to the era of photographic plates. Corliss & Bozman (1962) (hereafter CB) measured $\log gf$ values for Hf I and Hf II in arc spectra for a large number of lines over the wavelength interval 2000–9000 Å. Andersen et al. (1976) (hereafter APH) measured lifetimes for nine levels in Hf II using the beam-foil technique and rescaled the results of CB. The results of the two groups agree to within an uncertainty of typically 10% for the levels above 30 000 cm^{-1} but for lower levels they deviate considerably. However, the work of APH is limited to relatively few transitions at optical and near-IR wavelengths.

Our need for accurate oscillator strengths at UV wavelengths, to analyse spectra of warm stars, motivates the experimental work presented here.In this work we report radiative lifetimes of eight Hf I levels and 18 Hf II levels, measured with the laser induced fluorescence (LIF) technique. Branching fractions (*BF*s) for transitions from the Hf II levels have been measured from Fourier transform (FT) spectra. Combining the new lifetimes with the *BF*s, 195 absolute oscillator strengths have been derived. In addition to the *BF*s we have measured accurate wavelengths for the 195 Hf II lines. These data are applied to the determination of the hafnium abundance in the chemically peculiar stars χ Lupi (HgMn) and HR 3383 (hot-Am), and they are discussed in terms of possible revisions of the hafnium abundance for the Sun and the galactic halo stars CS 22892-052 and CS 31082-001.

2. Experimental work

2.1. Lifetime measurements

For the lifetime experiments we apply the LIF technique, as performed in previous experiments at the Lund Laser Centre. Free neutral and singly-ionised hafnium atoms were produced by laser ablation utilizing pulses from a Nd:YAG laser, characterised by a 532 nm wavelength, 10 Hz repetition rate, 10 ns duration and variable pulse energy (2−10 mJ). The laser pulses were focused onto the surface of a hafnium foil, which was rotating in a vacuum chamber with a pressure of about 10^{-6} mbar. In order to obtain the required excitation wavelengths during the LIF measurements a second injection-seeded and Q-switched Nd:YAG laser was used to pump a dye laser operated with the dye DCM. Before the pulses from the Nd:YAG laser were sent to the dye laser, they were shortened to about 1 ns in a watercell compressor based on stimulated Brillouin scattering. Depending on excitation wavelength for the investigated levels different non-linear processes were adopted to obtain UV radiation in the range 208 to 380 nm. The second harmonic of the dye laser was obtained in a KDP crystal. The third-order harmonic of the dye laser could be produced by mixing the second harmonic with the fundamental frequency of the dye laser in a BBO crystal. To extend the tuneable wavelength range further, the laser beam could be frequency shifted in a hydrogen cell using stimulated Raman scattering. The excitation beam was directed into the vacuum chamber and interacted with the ablated atoms and ions about 1 cm above the foil. The two Nd:YAG lasers were externally trigged by a delay generator, which enabled a free variation of the delay time between the ablation and excitation laser pulses. The fluorescence, released at the decay of the excited levels, was focused onto the entrance slit of a 1/8 m monochromator equipped with a micro-channel-plate photomultiplier tube (200 ps rise time). A transient digitizer was used to record and average the signals from the photomultiplier. Finally, the average time-resolved signals were transferred to a computer for the lifetime evaluations. For the shorter lifetimes the excitation pulse was also recorded and the lifetime was obtained in a deconvolution procedure, thus avoiding effects of the limited time response of the detection system. A more detailed discription of the setup can be found in Li et al. (2000).

The results of the lifetime measurements are presented in Table 3 for Hf I and Table 4 for Hf II.

2.2. Intensity and wavelength measurements

Hafnium spectra covering the wavenumber region 12 500 to 55 000 cm^{-1} (~1800–8000 Å) were recorded with the Chelsea instrument FT500 UV FT spectrometer at Lund Observatory using a resolution of 0.035 cm^{-1}. A water-cooled hollow cathode discharge with a cathode made out of a 5 cm long, 5 mm thick hafnium tube with a inner bore diameter of 2.5 mm was used as the light source. Spectra were recorded with discharge currents between 0.1 and 0.5 A, at an argon carrier gas pressure of 1.6 mbar. To derive relative intensities, the spectra were corrected for the instrumental response by using a tungsten ribbon lamp between 12 500 and 22 300 cm^{-1}, known Ar II brancing ratios from Whaling et al. (1993) between 20 000 to 30 000 cm^{-1}, and a deuterium lamp for wavenumbers above 27 800 cm^{-1}.

Hafnium has six naturally occurring stable isotopes (A = 174, 176, 177, 178, 179, 180), of which two are odd and might be expected to show hyperfine structure. None of these effects were resolved in the FT spectra, but many lines show asymmetric and broadened profiles as seen in Fig. 1. The broad foot on this particular line is one of the largest deviations from a Voigt profile seen in our data.

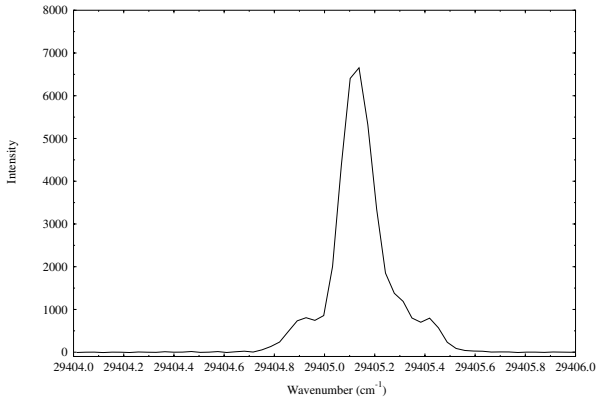

Fig. 1. The profile of the resonance line 5d6s^2 a^{2}D$_{3/2}$–5d6s (a^{3}D)6p z^{4}F$_{5/2}$ Hf II λ3399.790, showing effects of unresolved hyperfine structure and isotopic shift.

The BF of a line is derived by dividing the intensity of the line by the sum of the intensities of all lines coming from the same upper level,

$$(BF)_{ik} = A_{ik} / \sum_k A_{ik} = I_{ik} / \sum_k I_{ik}, \quad (1)$$

where A_{ik} is the transition probability of the line and I_{ik} is the intensity measured in photons per second. The line intensities were measured by integrating the area under the line profile. In practice, it may not be possible to measure all lines from an energy level, as some lines may be too weak or they may be located outside the recorded spectral region. The missing lines give rise to a residual intensity, which in this work was estimated with theoretical calculations made with the Cowan code (Cowan 1981). The calculated residual intensity is in most cases small, the largest being 5.6% (see Table 5).

Wavelengths for the Hf II lines were measured from the FT spectra using a center-of-gravity technique, since the line profiles are far from Voigt profiles no curve fitting was attempted. The spectra were wavelength calibrated by Ar II lines reported by Whaling et al. (1995). The line density of the hafnium spectra is high and some cases of line blending were seen. The 11 lines affected by line blending are marked in Table 5. The importance of the blends is reflected in the uncertainties attached to the gf value. The lines still having a small uncertainty are only blended with weak lines in either wing where the effect of the blend is small. A few lines are more severely blended and, therefore, have larger uncertainties.

2.3. Oscillator strengths

The transition probability (A-value) of a line can be derived from the relation:

$$A_{ik} = \frac{(BF)_{ik}}{\tau_i}, \quad (2)$$

where τ_i is the lifetime of the upper level. The oscillator strengths, or gf-values, are then derived from the A-value via the relation:

$$g_k f = 1.4992 \times 10^{-16} \lambda^2 g_i A_{ik}, \quad (3)$$

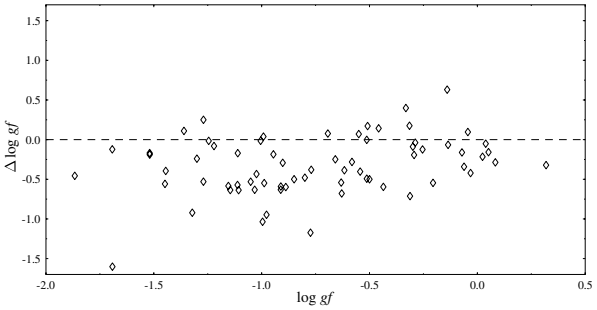

Fig. 2. Comparison of the oscillator strengths from Corliss & Bozman (1962) with the values derived in this work. $\Delta\log\, gf = \log gf_{\rm New} - \log gf_{\rm CB}$.

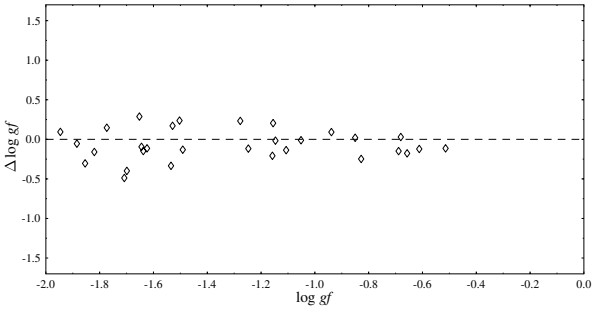

Fig. 3. Comparison of the oscillator strengths from Andersen et al. (1976) with the values derived in this work. $\Delta\log\, gf = \log gf_{\rm New} - \log gf_{\rm APH}$.

where λ is the wavelength in units of Å, A_{ik} is in s^{-1}, and g_i and g_k are the statistical weights for the upper and lower levels, respectively.

In Table 5 the BFs and log gf values are presented and compared with the values of APH and CB. In Figs. 2 and 3 the new log gf values are plotted against the difference between the new log gf values and the values determined by CB and APH, respectively. The comparison with the values of CB shows a large scatter with an offset of approximately −0.4. The comparison with APH in Fig. 3 shows a smaller scatter and the offset is only about −0.1. Andersen et al. rescaled the log gf values of CB using new lifetimes, but the uncertainty in the BF part is still present.

The total uncertainty presented in Table 5 is derived with contributions from the intensity measurements, the intensity calibration, the combination of different spectral regions, the self-absorption correction, the corrections for residuals and the lifetime measurements. The uncertainties are estimated as described in Sikström et al. (2002).

3. Astronomical applications

3.1. Chemically peculiar stars

We have investigated the hafnium abundance in two sharp-lined chemically peculiar (CP) stars, χ Lupi (=HD 141556, B9.5IVp HgMn + A2 Vm) and HR 3383 (=HD 72660, A1Vm), by fitting synthetic spectra to high-resolution ultraviolet spectra taken with the *Hubble Space Telescope* (*HST*). Both the HgMn and Am CP star classes are known to exhibit elemental abundances

that are enhanced above the solar system values. The determination of elemental abundances for χ Lupi A has been a focus of the χ Lupi Pathfinder project (Leckrone et al. 1999). For the heaviest stable elements the recent additions of osmium and iridium to the analysis of χ Lupi A has defined an enhancement peak that is comprised of the elements platinum, gold, mercury, and thallium (Ivarsson et al. 2004). Now, with the consideration of hafnium this project has realized defining the abundance distribution with the use of accurate atomic data for all stable elements heavier than the lanthanides ($72 \leq Z \leq 83$).

Spectral data for χ Lupi were obtained using the *HST* Goddard High Resolution Spectrograph (GHRS) and have been described by Brandt et al. (1999) and Leckrone et al. (1999). With only a limited spectral coverage we were fortunate to work with the line Hf II λ2683, which has the largest gf value in our laboratory sample. The FTS profile for this line is well fitted by a Voigt profile, and shows no effects of hyperfine or isotope structure, such as is observed for Hf II λ3399.790 (Fig. 1). Other lines of near comparable strength are either blended or do not exist in our GHRS dataset. Although three GHRS observations of χ Lupi were made at this wavelength setting, only one (Z28H010L) is useful for our purpose. The uncertainties in the companion star spectral synthesis preclude the use of the other two observations for analyzing this line.

The GHRS spectrum was analysed in a manner similar to previously published results. Model atmospheres created with the ATLAS9 code (Kurucz 1993a) with model parameters ($T_{\rm eff}$ = 10 650 K, $\log g$ = 3.8, $\xi_{\rm t}$ = 0.0 km s^{-1}, $v \sin i$ = 1.0 km s^{-1} for the primary star and $T_{\rm eff}$ = 9200 K, $\log g$ = 4.2, $\xi_{\rm t}$ = 2.0 km s^{-1}, $v \sin i$ = 2.0 km s^{-1} for the secondary) were used in the SYNTHE (Kurucz 1993b) synthetic spectrum code. Atomic line data were taken from the compilation of Kurucz (1993b) with the exception of data discussed in this work. Elemental abundances for elements other than hafnium were taken from Leckrone et al. (1999). The computed spectra were coadded, taking into account the wavelength dependent luminosity ratio ($L_{\rm pri}/L_{\rm sec}$ = 5.67) and the wavelength shift between the components ($\Delta\lambda = \lambda_{\rm pri} - \lambda_{\rm sec}$ = −0.637 Å) at the time of the observation, based upon the ephemeris of Dworetsky (1972). The resulting spectrum was convolved with the instrument broadening function, modeled as a Gaussian of resolving power R = 86 560 for the relevant echelle order, and placed on the laboratory wavelength scale by shifting the observed spectrum to match spectral features of iron-group elements. Figure 4 presents the comparison of the observation with synthetic spectra computed for hafnium enhancements of [Hf/H] = $\log \epsilon$(Hf)$_{\rm star}$ − $\log \epsilon$(Hf)$_{\rm Sun}$ = 0.0, 1.0, 1.3, and 1.5 dex. We adopt [Hf/H] = 1.3, though the value should be considered an upper limit due to data noise (maximum S/N = 140), small uncertainties in the luminosity ratio, and unknowns regarding certain elemental abundances for the secondary star. The feature at this wavelength does not appear to be an instrument artifact.

High-resolution ultraviolet spectra of the hot-Am star HR 3383 were taken with the *HST* Space Telescope Imaging Spectrograph (STIS) (*HST* Prop GO9455, PI R. Peterson). The data, extracted from the *HST* data archive MAST and reduced by the STIS team at Goddard Space Flight Center (private communication), have a nominal resolving power of $R = \lambda/\Delta\lambda$ = 114 000, and display a typical S/N of near 100. Three spectral images were utilized in this analysis (ID numbers O6LM51030, O6LM51010, O6LM51020) that span the wavelength region 2128−2888 Å.

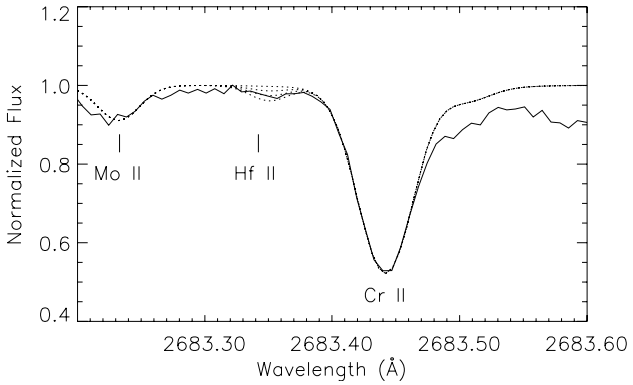

Fig. 4. Spectrum fitting for Hf II λ2683.3443 in χ Lupi. The observation (solid) is compared with synthetic spectra (dotted) computed for hafnium abundance enhancements of [Hf / H] = 0.0, 1.0, 1.3, 1.5 dex.

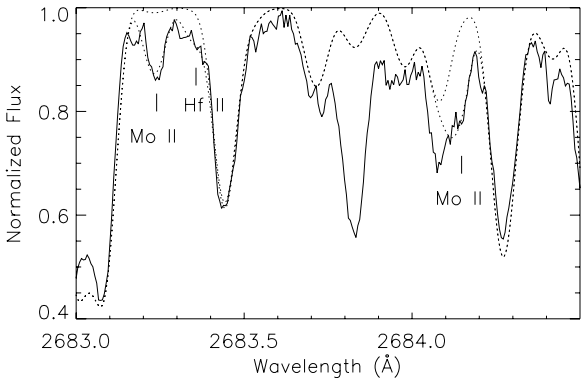

Fig. 5. Synthetic spectrum fitting for HR 3383. The observation (solid) is compared with synthetic spectra (dotted) computed for abundance enhancements of hafnium [Hf/H] = 0.0, 1.7 dex and molybdenum [Mo/H] = 0.0, 1.2 dex. The strong central feature not present in the synthetic spectrum is unidentified.

Synthetic spectra for HR 3383 were computed with the SYNTHE code, using an ATLAS9 model atmosphere for the atmospheric parameters $T_{\rm eff}$ = 9750, $\log g$ = 4.0, $\xi_{\rm t}$ = 0.0 km s^{-1}. A rotational velocity ($v \sin i$) of 5.5 km s^{-1} was determined from the data, which is lower than the 6.5 km s^{-1} value of Adelman et al. (2004). This difference is attributed to the higher resolving power of the STIS long wavelength spectra relative to the data used at shorter wavelengths, which allowed us to determine a lower rotational velocity.

From our experimental line sample (Table 5) only two Hf II lines, λ2683.39 and the weaker λ2820.225, were detected in the stellar spectrum. For the former, Fig. 5 presents a comparison of the HR 3383 observation with synthetic spectra computed for the solar abundance and an enhancement over the solar value of [Hf/H] = 1.7 dex. This enhancement yields a best fit to the spectrum to within an uncertainty of ±0.2 dex for the

Table 1. Hf II lines in HR 3383.

λ_{air} (Å)	log gf CB	log gf New	log $\epsilon_r m$(Hf)
2641.410	+0.67		2.19
2647.297	+0.46		2.14
2683.349	+0.64	+0.319	2.54
2773.356	+0.21		2.54
2774.014	–0.28		2.64
2820.225	–0.14	–0.044	2.64

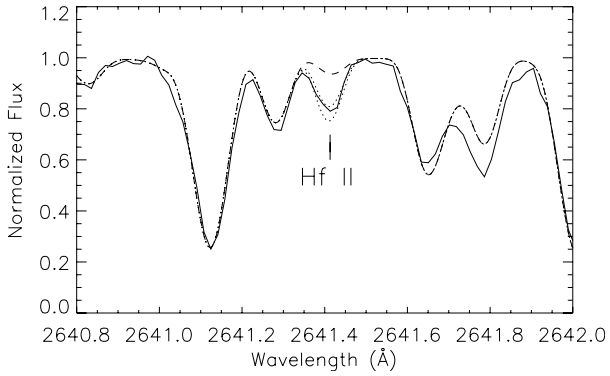

Fig. 6. Hf II λ2641.4 in the spectrum of HR 3383. The observation (solid) is compared with synthetic spectra computed for hafnium abundance enhancements of [Hf/H] = 0.0 (dashed) and +1.3, 1.5 dex (dotted).

combination of R and $v \sin i$ specified above, and our placement of the continuum.

To achieve the best fit the observed spectrum was shifted by −0.840 Å to place it on the laboratory rest frame. As a result of noise an uncertainty of ±0.004 Å is tolerated to fit many of the spectral features. The absolute wavelength scale was set by the Cr II λ2683.443 line, as its wavelength has been measured by FT spectroscopy to an uncertainty of approximately 1 mÅ. The continuum level was set by matching the high points in the spectrum found within several angstroms of the Hf II line. The uncertainty in the continuum placement is between 1−2%. The Hf II λ2683 line serves as the main indicator of the hafnium abundance in this star due to the nature of the atomic data.

Four Hf II lines from the list of CB have also been incorporated into this analysis of the Hf II spectrum. All lines are located longward of 2600 Å, and thus avoid the most severe regions of line blending. Table 1 presents the oscillator strengths and derived abundances for the six lines used in the analysis of HR 3383. Abundances quoted are for the new gf values when a line has an entry from CB. Figure 6 presents the comparison between observed and synthetic spectra for one of these lines, Hf II λ2641.410, which is the most prominent of the Hf II lines we have studied. Two of these lines yield an abundance for hafnium that is similar to that determined from the new line data, and two result in a noticeably lower abundance. There is a high likelihood that the oscillator strengths from CB are systematically higher than would be determined by modern techniques, such as the LIF method employed here. If corrected, this would lead to a somewhat higher abundance. This possibility is borne out by our comparison of gf values between CB and this study, as presented in Fig. 2.

Table 2. Rescaled abundances in CS 22892-052 and CS 31082-001.

λ (Å)	log gf APH[a]	log gf New	log ϵ(Hf) Prev.[b]	log ϵ(Hf) New
CS 22892-052				
3719.273	–0.87	–0.850	–0.8	–0.82
3793.373	–0.95	–1.158	–1.0	–0.81
CS 31082-001				
3399.790	–0.49	–0.612	–0.90[c]	–0.78
3719.273	–0.87	–0.850	–0.70	–0.72

[a] Andersen et al. (1976).
[b] Sneden et al. (1996) for CS 22892-052 and Hill et al. (2002) for CS 31082-001.
[c] From Fig. 6 Hill et al. (2002).

In the course of our work on Hf II we became aware of two obvious lines of Mo II in the spectrum of HR 3383. These lines are noted in Fig. 5. A search for other Mo II lines of comparable strength showed them to be blended. The abundance of molybdenum was determined for HR 3383 using the wavelength and oscillator strength data of Sikström et al. (2001). A best fit was obtained for an abundance of log ϵ(Mo) = +3.1 dex, which is an enhancement of +1.2 dex over the solar abundance. The abundance of molybdenum in χ Lupi A has been reported by Leckrone et al. (1999) to be log ϵ(Mo) = 2.90.

3.2. The metal-poor halo stars CS 22892-052 and CS 31082-001

The new Hf II gf values can be applied to previous abundance analyses of metal-poor halo stars. By scaling the former abundances by the ratio of the old to new gf values we can adjust the hafnium abundance in these stars and attempt to reconcile abundance differences with the scaled solar r-process models. For the two lines used by Sneden et al. (1996) in the analysis of CS 22892-052 new gf values give a narrowing of the 1σ uncertainty from 0.14 to 0.007 and increases the abundance from log ϵ = −0.90 to log ϵ = −0.82 (see details in Table 2). In the more recent work by Sneden et al. (2003), where the stated abundance is log ϵ = −0.98 ± 0.10, the abundance from each line is not presented, but if the difference is the same in both lines it would mean that the abundance after scaling with the new gf values remains at log ϵ = −0.90.

In applying the same approach to the results of Hill et al. (2002) on CS 31082-001 a descrepancy appears. The previously derived abundance from the Hf II λ3399.273 line is log ϵ = −0.5 and would increase to −0.38 after the new gf value is substituted for the old one, while the abundance for the line λ3719.273 stays almost the same (log ϵ = −0.70 changes to −0.72), resulting in an increase in the uncertainty. Figure 6 in Hill et al. (2002) shows synthetic spectrum fits to the λ3399.273 line for three different abundances. It is suspected that the final abundance has been misquoted in their text, since, in their figure it is clear that the synthetic spectrum with an abundance of log ϵ = −0.90, and not the spectrum with log ϵ = −0.50, has the best fit. This would explain the

discrepancy with the 1σ uncertainty becoming larger and would instead decrease it to 0.04. In Table 2 the abundance read from the figure is used to show what their abundance would be if it were scaled using the new log gf values. The hafnium abundance in CS 31082-001 then becomes $\log \epsilon = -0.75$. Applying the re-evaluated hafnium abundance to the comparison Hill et al. (2002) makes between the abundances in CS 31082-001 and scaled solar *r*-process abundances, shifts the hafnium point towards the solar *r*-process pattern strengthening the fit to it. It should be noted that using the abundance derived from Fig. 6 in Hill et al. (2002) gives a value slightly closer to the solar *r*-process pattern, with the log gf values of Andersen et al. (1976), than with the new values from this work, although the uncertainty decreases with the new values.

4. Results and conclusion

Wavelengths and oscillator strengths for 195 lines of the Hf II spectrum have been derived from experiments by combining lifetimes and *BF*s of 18 levels. Additionally, new measured lifetimes for 8 levels in Hf I are presented.

With these new data the abundance of hafnium for two CP stars has been determined, which both extends our knowledge of heavy element abundances and highlights an interesting difference. For χ Lupi A the hafnium abundance derived here is consistent with previous results for the heavy elements tantalum, tungsten, rhenium, osmium, iridium, lead, and bismuth in that we have determined an abundance enhancement, or upper limit, at the enhancement level of approximately 1 dex. By contrast, the elements platinum, gold, mercury, and thallium stand out as enhanced by more than four orders of magnitude.

The somewhat cooler Am star HR 3383 has been documented as having an enhancement of gold of +1.9 dex (Adelman et al. 2004), which is similar to the hafnium enhancement presented here (+1.7 dex). Spectral lines of other platinum-group elements have also been detected by us in the UV spectrum of HR 3383 (work in progress) and point to similar enhancements. Therefore, over a short span of spectral type (B9.5 to A1) there exists a remarkably different behaviour for the heaviest elements, with certain of them having a tendancy for extreme enhancements. One caveat to these results is that we assume that the hafnium isotope composition for these two stars is also solar-like. We are unable to derive any isotope composition information from the data. Evidence for isotope anomalies in HgMn stars is common, and suspected for hot-Am stars. Therefore, if the isotope composition differs from that of the Sun, then the abundances must be adjusted.

Rescaling the hafnium abundances in the metal-poor halo stars CS 22892-052 (Sneden et al. 1996) and CS 31082-001 (Hill et al. 2002) with the new log gf values decreases the 1σ uncertainty of the result in both stars considerably. In CS 22892-052 the rescaled abundance becomes $\log \epsilon = -0.82$, or $\log \epsilon = -0.90$ if assuming the abundance of Sneden et al. (2003), with 1σ uncertainty of 0.007. The lack of infromation on individual lines of Hf II used by Sneden et al. (2003) precludes us from choosing between those two values. In CS 31082-001 the rescaled abundance becomes $\log \epsilon = -0.75$, using the abundance of Fig. 6 in Hill et al. (2002), 1σ uncertainty of 0.04. The re-evaluated abundance of CS 31082-001 now better fits the scaled solar *r*-process pattern, which together with the recently updated abundance for osmium (Ivarsson et al. 2003) strengthening the theory of an universal *r*-process in the early galaxy.

Comparison of the gf values for Hf II presented here with those of APH suggests that the solar hafnium abundance may be underestimated by between 0.1 and 0.2 dex. Two of the six lines (Hf II $\lambda\lambda$3253.70, 3535.54) used by APH are found by us to have log gf values more negative, by amounts of 0.25 and 0.15 dex, respectively. For a similar abundance analysis procedure, where we would substitute our gf values for those of APH, this would imply that the solar abundance is approximately 0.2 dex larger than their derived value. Three other lines considered by APH are also in our dataset, with two of them ($\lambda\lambda$3399.790, 3569.034) now having lower log gf values by 0.12 dex. The third line (λ3719.273) has a similar gf value in both studies. However, these three lines were not used by APH in their final abundance determination as a result of severe line blending. For these five lines in common to both studies, the average difference between the new and APH log gf values is −0.12 dex. From Fig. 3 we show that other lines in our comparison samples are, on average, systematically of lower log gf value than those of APH. Therefore, we conclude that the canonical solar photospheric hafnium abundance should be rescaled upwards, to a value near $\log \epsilon(\mathrm{Hf}) = +1.0$. We hesitate to assign stringent uncertainties to this number, since considerable uncertainty can arise from the continuum placement in the analysis of the solar spectrum, as pointed out by APH. The uncertainties of the gf values for our data are at the 10−20% level for the lifetime measurements, which are marginally lower uncertainties than those quoted by APH. An interesting result of increasing the solar photospheric hafnium abundance is to increase the discrepancy between the solar system hafnium abundance as determined from chondritic meteorites ($\log \epsilon(\mathrm{Hf}) = +0.77 \pm 0.04$ (Lodders 2003) and our suggestion of a rescaling of the photosphere value ($\log \epsilon(\mathrm{Hf}) = +1.0$).

Acknowledgements. We would like to thank the Lund Laser Center for providing time to conduct this experiment. Some of the data presented in this paper were obtained from the Multimission Archive at the Space Telescope Science Institute (MAST). STScI is operated by the Association of Universities for Research in Astronomy, Inc., under NASA contract NAS5-26555. Support for MAST for non-HST data is provided by the NASA Office of Space Science via grant NAG5-7584 and by other grants and contracts.

References

Adelman, S. J., Proffitt, C. R., Wahlgren, G. M., Leckrone, D. S., & Dolk, L. 2004, ApJS, 155, 179
Andersen, T., Petersen, P., & Hauge, O. 1976, Sol. Phys., 49, 211
Brandt, J. C., Heap, S. R., Beaver, E. A., et al. 1999, AJ, 117, 1505
Corliss, C. H., & Bozman, W. R. 1962, NBS Monograph, 53
Cowan, R. D. 1981, The Theory of Atomic Structure and Spectra (Berkley, CA: University of California)
Cowley, C. R., Ryabchikova, T., Kupka, F., et al. 2000, MNRAS, 317, 299

Duquette, D. W., Salih, S., & Lawler, J. E. 1982, Phys. Rev. A, 26, 2623
Dworetsky, M. M. 1972, PASP, 84, 254
Hill, V., Plez, B., Cayrel, R., et al. 2002, A&A, 387, 560
Ivarsson, S., Andersen, J., Nordström, B., et al. 2003, A&A, 409, 1141
Ivarsson, S., Wahlgren, G. M., Dai, Z., Lundberg, H., & Leckrone, D. S. 2004, A&A, 425, 353
Kurucz, R. 1993a, ATLAS9 Stellar Atmosphere Programs and 2 km s^{-1} grid, Kurucz CD-ROM No. 13, Cambridge, Mass.: Smithsonian Astrophysical Observatory, 13
Kurucz, R. 1993b, SYNTHE Spectrum Synthesis Programs and Line Data, Kurucz CD-ROM No. 18, Cambridge, Mass.: Smithsonian Astrophysical Observatory, 18
Leckrone, D. S., Proffitt, C. R., Wahlgren, G. M., Johansson, S. G., & Brage, T. 1999, AJ, 117, 1454
Li, Z. S., Lundberg, H., Wahlgren, G. M., & Sikström, C. M. 2000, Phys. Rev. A, 62, 032505
Lodders, K. 2003, ApJ, 591, 1220
Moore, C. E. 1952, Atomic Energy Levels Natl. Bur. Stand. (US) Circ. 467, Vol. II
Reynolds, S. E., Hearnshaw, J. B., & Cottrell, P. L. 1988, MNRAS, 235, 1423
Sikström, C. M., Pihlemark, H., Nilsson, H., et al. 2001, J. Phys. B Atom. Molec. Phys., 34, 477
Sikström, C. M., Nilsson, H., Litzén, U., Blom, A., & Lundberg, H. 2002, J. Quant. Spec. Radiat. Transf., 74, 355
Sneden, C., Cowan, J. J., Lawler, J. E., et al. 2003, ApJ, 591, 936
Sneden, C., McWilliam, A., Preston, G. W., et al. 1996, ApJ, 467, 819
Whaling, W., Anderson, W. H. C., Carle, M. T., Brault, J. W., & Zarem, H. A. 1995, J. Quant. Spec. Radiat. Transf., 53, 1
Whaling, W., Carle, M. T., & Pitt, M. L. 1993, J. Quant. Spec. Radiat. Transf., 50, 7
Wyart, J. F., & Blaise, J. 1990, Phys. Scr., 42, 209
Yushchenko, A., Gopka, V., Goriely, S., et al. 2005a, A&A, 430, 255
Yushchenko, A., Gopka, V., Kim, C., et al. 2005b, MNRAS, 359, 865

Online Material

Table 3. Experimental radiative lifetimes of Hf I.

Configuration[a]	Energy	J	$\lambda^b_{\rm exc}$	$\lambda^c_{\rm obs}$	Exp. lifetime (ns)	
	cm^{-1}		(Å)	(Å)	This work	DSL[d]
$5d^26s(a^4P)6p\ y^5D^o$	31 342.51	3	3190.55	3730	63.5(4.5)	62.3(3.1)
$5d^26s(b^2D)6p\ z^1D^o$	31 610.80	2	3163.48	3850	19.3(1.7)	18.7(0.9)
$5d^26s(a^4P)6p\ z^5P^o$	33 121.48	2	3250.47	3020	15.3(1.5)	
	33 538.15	2	3207.03	2980	11.2(1.1)	
	34 877.04	3	2867.22	2870	5.7(0.7)	
	46 170.12	2	2165.90	3180	12.2(1.2)	
	46 775.98	3	2137.85	2760	13.0(1.2)	
	47 590.09	3	2101.28	3240	6.7(0.5)	

[a] Notation from Moore (1952).
[b] Laser wavelength used to populate the upper state.
[c] Wavelength used to detect the fluorescence signal.
[d] DSL = Duquette et al. (1982).

Table 4. Experimental radiative lifetimes of Hf II.

Configuration[a]	Energy	J	$\lambda^b_{\rm exc}$	$\lambda^c_{\rm obs}$	Exp. lifetime (ns)	
	cm^{-1}		(Å)	(Å)	This work	APH[d]
$5d6s(a^3D)6p\ z^4F^o$	29 405.129	2.5	3794.46	3400	29.7(2.4)	21(3)
	33 776.300	3.5	3254.64	3650	34.8(2.5)	23(3)
$5d6s(a^3D)6p\ z^4D^o$	31 784.202	1.5	3146.22	3720	21.8(1.8)	20(3)
	34 355.172	2.5	2910.77	3570	16.2(1.4)	14.5(2.0)
$5d6s(a^1D)6p\ z^2D^o$	33 180.970	2.5	3318.99	3010	18.1(1.5)	16(2)
	34 123.965	1.5	3218.22	3280	24.5(2.5)	
$5d^2\ (a^3F)6p\ z^4G^o$	34 942.411	2.5	3195.12	3500	8.4(0.5)	
	38 498.566	3.5	2821.06	3110	5.1(0.3)	
$5d^2\ (a^3F)6p\ y^4F^o$	42 518.148	1.5	2351.94	2530	2.3(0.2)	
	43 680.787	2.5	2289.34	5650	3.3(0.2)	
$5d6s(a^1D)6p\ y^2P^o$	42 770.596	1.5	2338.06	2520	2.6(0.2)	
	43 044.258	0.5	2323.19	2540	1.8(0.2)	
$5d^2\ (a^3F)6p\ y^4D^o$	45 643.263	0.5	2190.90	2970	2.2(0.2)	
	46 674.354	1.5	2142.50	2390	2.1(0.2)	
	47 904.443	2.5	2087.49	3810	2.0(0.2)	
$5d^2\ (a^3P)6p\ z^2S^o$	46 495.401	0.5	2150.75	3200	2.7(0.2)	
$5d^2\ (a^3F)6p\ z^2G^o$	49 840.585	4.5	2299.06	3080	3.1(0.2)	
$5d^2\ (a^3F)6p\ x^2F^o$	52 340.079	3.5	2108.04	2680	1.9(0.2)	

[a] Notation from Wyart & Blaise (1990).
[b] Laser wavelength used to populate the upper state.
[c] Wavelength used to detect the fluorescence signal.
[d] APH = Andersen et al. (1976).

Table 5. Hf II branching fractions (BFs) and log gf-values sorted by upper level.

Upper level[a] $(cm)^{-1}$	Lower level $(cm)^{-1}$	λ_{Air} (Å)	σ $(cm)^{-1}$	BF[b]	gf	log gf This work	log gf APH[c]	log gf CB[d]	Unc. (% in gf)
29405.129	15 084.288	6980.901	14 320.849	0.010	0.015	–1.820	–1.66		23
$\tau = 29.7ns$	14 359.454	6644.592	15 045.677	0.010	0.014	–1.854	–1.55		23
$J = 2.5$	13 485.554	6279.844	15 919.558	0.002	0.003	–2.541			22
	12 070.491	5767.199	17 334.634	0.003	0.003	–2.531	–2.26		21
	6344.381	4335.154	23 060.746	0.003	0.002	–2.822			22
	4904.869	4080.437	24 500.261	0.050	0.025	–1.596			24
	3644.633	3880.813	25 760.493	0.064	0.029	–1.535	–1.20		27
SA	3050.863	3793.373	26 354.278	0.159	0.070	–1.158	–0.95		25
SA	0.00	3399.790	29 405.145	0.697	0.244	–0.612	–0.49		11
				0.000					
31784.202	15 254.338	6047.994	16 529.832	0.002	0.002	–2.705			18
$\tau = 21.5ns$	12 920.933	5299.831	18 863.276	0.005	0.004	–2.376			19
$J = 1.5$	12 070.491	5071.200	19 713.702	0.003	0.002	–2.665			40[e]
	11 951.660	5040.812	19 832.542	0.044	0.031	–1.503	–1.74		20
	4904.869	3719.273	26 879.333	0.366	0.141	–0.850	–0.87		14
	3644.633	3552.700	28 139.564	0.222	0.078	–1.107	–0.97		17
	3050.863	3479.281	28 733.349	0.263	0.089	–1.052	–1.04		16
	0.00	3145.305	31 784.216	0.086	0.024	–1.624	–1.51		19
				0.004					
33180.970	15 084.288	5524.343	18 096.675	0.011	0.017	–1.773	–1.92		21
$\tau = 18.1ns$	14 359.454	5311.594	18 821.506	0.038	0.053	–1.277	–1.51		20
$J = 2.5$	13 485.554	5075.910	19 695.413	0.004	0.005	–2.270			17
	12 920.933	4934.449	20 260.033	0.018	0.022	–1.652	–1.94		19
	12 070.491	4735.663	21 110.460	0.004	0.004	–2.375			16
	4904.869	3535.546	28 276.095	0.329	0.205	–0.689	–0.54		15
	3644.633	3384.690	29 536.326	0.034	0.020	–1.708	–1.22		19
	3050.863	3317.984	30 130.111	0.059	0.032	–1.491	–1.36		20
	0.00	3012.897	33 180.978	0.462	0.209	–0.681	–0.71		14
				0.040					
33776.300	17 710.820	6222.810	16 065.466	0.003	0.004	–2.437			17
$\tau = 34.8ns$	17 368.915	6093.122	16 407.406	0.002	0.002	–2.632			17
$J = 3.5$	15 084.288	5348.390	18 692.015	0.006	0.006	–2.255			18
	13 485.554	4926.981	20 290.741	0.006	0.005	–2.318			19
	12 070.491	4605.774	21 705.796	0.018	0.013	–1.885	–1.83		20
	8361.846	3933.655	25 414.453	0.029	0.015	–1.813			17
	6344.381	3644.350	27 431.915	0.481	0.220	–0.657	–0.48		12
	4904.869	3462.640	28 871.431	0.048	0.020	–1.699	–1.30		19
	3050.863	3253.693	30 725.446	0.407	0.149	–0.828	–0.58		15
				0.001					
34123.965	15 254.338	5298.049	18 869.622	0.078	0.054	–1.270		–1.52	21
$\tau = 24.5ns$	14 359.454	5058.164	19 764.509	0.007	0.004	–2.348			19
$J = 1.5$	13 485.554	4843.981	20 638.409	0.010	0.006	–2.223			18
	12 920.933	4714.987	21 203.034	0.003	0.002	–2.731			18
	12 070.491	4533.163	22 053.467	0.043	0.022	–1.662			19

Table 5. continued.

Upper level[a] $(cm)^{-1}$	Lower level $(cm)^{-1}$	λ_{Air} (Å)	σ $(cm)^{-1}$	BF[b]	gf	log gf This work	log gf APH[c]	log gf CB[d]	Unc. (% in gf)
	11 951.660	4508.871	22 172.284	0.001	0.0003	–3.478			17
	4904.869	3421.437	29 219.104	0.022	0.006	–2.197		–1.87	20
	3644.633	3279.967	30 479.329	0.228	0.060	–1.221		–1.14	18
	3050.863	3217.287	31 073.114	0.119	0.030	–1.519		–1.35	21
	0.00	2929.633	34 123.981	0.485	0.102	–0.992		–1.03	14
				0.002					
34355.172	15 084.288	5187.738	19 270.858	0.020	0.030	–1.529	–1.70		20
$\tau = 16.2ns$	14 359.454	4999.676	19 995.716	0.008	0.011	–1.946	–2.04		20[e]
$J = 2.5$	12 920.933	4664.127	21 434.238	0.058	0.070	–1.155	–1.36		16
	12 070.491	4486.130	22 284.675	0.021	0.023	–1.638	–1.49		18
	6344.381	3569.034	28 010.790	0.432	0.306	–0.514	–0.40		12
	4904.869	3394.576	29 450.305	0.111	0.071	–1.147	–1.13		18
	3644.633	3255.273	30 710.536	0.096	0.057	–1.247	–1.13		20
	3050.863	3193.524	31 304.321	0.203	0.115	–0.939	–1.03		17
	0.00	2909.917	34 355.184	0.048	0.023	–1.645	–1.55		20
				0.002					
34942.411	18 897.640	6230.834	16 044.778	0.002	0.010	–1.985			16
$\tau = 8.4ns$	17 830.392	5842.220	17 112.039	0.006	0.020	–1.693		–1.57	16
$J = 2.5$	17 710.827	5801.680	17 231.608	0.002	0.006	–2.221			17
	15 084.288	5034.317	19 858.130	0.001	0.004	–2.433			15
	14 359.454	4857.029	20 582.967	0.0001	0.0003	–3.511			14
	13 485.554	4659.204	21 456.888	0.003	0.006	–2.211			16
	12 920.933	4539.757	22 021.436	0.001	0.003	–2.564			17
	12 070.491	4370.945	22 871.921	0.038	0.077	–1.111		–0.94	17
	6344.381	3495.743	28 598.039	0.076	0.099	–1.005		–0.99	18
	4904.869	3328.209	30 037.553	0.026	0.030	–1.519		–1.33	20
	3644.633	3194.191	31 297.783	0.283	0.310	–0.509		–0.68	17
	3050.863	3134.717	31 891.570	0.331	0.349	–0.458		–0.60	15
SA	0.00	2861.009	34 942.439	0.231	0.203	–0.693		–0.77	20
				0.000					
38498.566	20 134.976	5444.046	18 363.587	0.006	0.044	–1.360		–1.47	19
$\tau = 5.1ns$	17 710.827	4809.186	20 787.729	0.001	0.007	–2.163			15
$J = 3.5$	17 368.915	4731.360	21 129.663	0.010	0.050	–1.300		–1.06	19
	15 084.288	4269.695	23 414.286	0.010	0.044	–1.352			20
	13 485.554	3996.786	25 013.029	0.007	0.028	–1.555			19
	12 070.491	3782.780	26 428.080	0.011	0.036	–1.445		–1.05	19
	8361.846	3317.257	30 136.718	0.002	0.006	–2.251			18
	6344.381	3109.112	32 154.196	0.227	0.515	–0.288		–0.25	18
	4904.869	2975.879	33 593.713	0.241	0.502	–0.299		–0.21	17
SA	3050.863	2820.225	35 447.726	0.483	0.904	–0.044		–0.14	13
				0.002					
42518.148	20 134.976	4466.389	22 383.172	0.018	0.095	–1.024		–0.59	19
$\tau = 2.3ns$	18 897.640	4232.386	23 620.681	0.050	0.234	–0.631		–0.09	19
$J = 1.5$	17 830.392	4049.446	24 687.760	0.018	0.077	–1.112		–0.54	19
	17 368.915	3975.139	25 149.238	0.005	0.020	–1.697			18

Table 5. continued.

Upper level[a] $(cm)^{-1}$	Lower level $(cm)^{-1}$	λ_{Air} (Å)	σ $(cm)^{-1}$	BF^b	gf	log gf This work	APH[c]	CB[d]	Unc. (% in gf)
	15 254.338	3666.819	27 263.826	0.005	0.017	–1.766			21
	14 359.454	3550.285	28 158.712	0.001	0.004	–2.358			17
	13 485.554	3443.418	29 032.588	0.001	0.003	–2.580			17
	12 070.491	3283.379	30 447.656	0.013	0.036	–1.448		–0.89	20
	4904.869	2657.844	37 613.290	0.068	0.125	–0.902		–0.61	21
SA	3644.633	2571.675	38 873.522	0.492	0.848	–0.071		0.09	15
	3050.863	2532.981	39 467.315	0.006	0.010	–2.004		–0.98	18
SA	0.00	2351.216	42 518.173	0.323	0.466	–0.331		–0.73	19
				0.000					
42770.596	20 134.976	4416.575	22 635.620	0.001	0.006	–2.257			18
$\tau = 2.6ns$	18 897.640	4187.663	23 872.941	0.012	0.048	–1.322		–0.40	19
$J = 1.5$	17 830.392	4008.461	24 940.178	0.016	0.058	–1.233			22
	17 368.915	3935.634	25 401.674	0.034	0.123	–0.911		–0.28	23
	15 254.338	3633.183	27 516.231	0.013	0.040	–1.403			21
	14 359.454	3518.741	28 411.130	0.045	0.129	–0.888		–0.29	20
	13 485.554	3413.734	29 285.036	0.027	0.072	–1.146		–0.51	22
	12 920.933	3349.161	29 849.646	0.009	0.024	–1.623			21
	3050.863	2516.882	39 719.738	0.748	1.093	0.039		0.09	9
	0.00	2337.338	42 770.603	0.045	0.057	–1.245		–1.23	21
				0.050					
43044.258	26 996.382	6229.629	16 047.880	0.003	0.020	–1.705			23
$\tau = 1.8ns$	18 897.640	4140.198	24 146.622	0.003	0.008	–2.113			22
$J = 0.5$	17 830.392	3964.949	25 213.872	0.039	0.103	–0.988		–0.44	25
	15 254.338	3597.401	27 789.917	0.049	0.105	–0.977		–0.03	22[e]
	14 359.454	3485.170	28 684.796	0.010	0.021	–1.688			22
	12 920.933	3318.730	30 123.337	0.003	0.006	–2.232			23
	11 951.660	3215.266	31 092.646	0.003	0.005	–2.310			22
	3644.633	2537.333	39 399.627	0.083	0.089	–1.051		–0.52	24
SA	0.00	2322.476	43 044.281	0.806	0.725	–0.140		–0.77	12
				0.001					
43680.787	28 458.225	6567.393	15 222.537	0.005	0.053	–1.274			16
$\tau = 3.3ns$	21 638.008	4535.363	22 042.771	0.013	0.074	–1.133			15
$J = 2.5$	20 134.976	4245.845	23 545.808	0.014	0.070	–1.154		–0.57	17
	18 897.640	4033.860	24 783.146	0.011	0.049	–1.314			23[e]
	17 830.392	3867.316	25 850.397	0.042	0.170	–0.770		–0.39	16
	17 710.827	3849.511	25 969.959	0.126	0.509	–0.293		–0.10	16
	15 084.288	3495.931	28 596.501	0.066	0.220	–0.659		–0.41	17
	13 485.554	3310.827	30 195.241	0.018	0.054	–1.270		–0.74	18
	12 920.933	3250.053	30 759.854	0.001	0.004	–2.397			14
	12 070.491	3162.612	31 610.285	0.062	0.168	–0.774		0.40	51[e]
	6344.381	2677.554	37 336.422	0.007	0.014	–1.866		–1.41	17
	4904.869	2578.148	38 775.924	0.133	0.242	–0.617		–0.23	17
SA	3644.633	2496.989	40 036.155	0.154	0.262	–0.581		–0.30	19
SA	3050.863	2460.495	40 629.941	0.337	0.557	–0.254		–0.13	15
	0.00	2288.627	43 680.850	0.002	0.003	–2.544			44[e]
				0.009					

Table 5. continued.

Upper level[a] $(cm)^{-1}$	Lower level $(cm)^{-1}$	λ_{Air} (Å)	σ $(cm)^{-1}$	BF^b	gf	log gf This work	APH[c]	CB[d]	Unc. (% in gf)
45643.263	26 996.382	5361.350	18 646.833	0.006	0.025	–1.608			17
$\tau = 2.2ns$	18 897.640	3737.869	26 745.608	0.192	0.367	–0.436		0.16	14[e]
$J = 0.5$	17 830.392	3594.435	27 812.847	0.011	0.019	–1.726			18
	15 254.338	3289.725	30 388.922	0.017	0.024	–1.611			17
	14 359.454	3195.621	31 283.777	0.067	0.093	–1.032		–0.40	18[e]
	11 951.660	2967.233	33 691.588	0.238	0.286	–0.543		–0.14	17
	3644.633	2380.305	41 998.619	0.397	0.307	–0.513		–0.51	14
	0.00	2190.218	45 643.278	0.069	0.045	–1.345			19
				0.003					
46495.401	27 285.047	5204.080	19 210.343	0.002	0.006	–2.195			12
$\tau = 2.7ns$	26 996.382	5126.812	19 499.866	0.013	0.037	–1.437			58[e]
$J = 0.5$	18 897.640	3622.451	27 597.752	0.040	0.058	–1.233			17
	17 830.392	3487.576	28 665.007	0.117	0.159	–0.800		–0.32	17
	15 254.338	3199.991	31 241.056	0.207	0.235	–0.629		0.05	15
	14 359.454	3110.877	32 135.953	0.286	0.307	–0.513		–0.02	14
	12 920.933	2977.584	33 574.472	0.125	0.123	–0.911		–0.32	18
	11 951.660	2894.037	34 543.678	0.018	0.017	–1.770			18
	3644.633	2332.965	42 850.770	0.187	0.113	–0.946		–0.76	16
	0.00	2150.072	46 495.431	0.005	0.003	–2.568			15
				0.000					
46674.354	28 546.991	5514.988	18 127.371	0.006	0.049	–1.313			18
$\tau = 2.1ns$	27 285.047	5156.049	19 389.295	0.003	0.026	–1.583			16
$J = 1.5$	26 996.382	5080.411	19 677.963	0.005	0.040	–1.393			16
	20 134.976	3766.916	26 539.377	0.154	0.623	–0.206		0.34	14[e]
	18 897.640	3599.111	27 776.711	0.028	0.104	–0.981			18
	17 830.392	3465.938	28 843.954	0.005	0.017	–1.778			17
	15 254.338	3181.762	31 420.036	0.008	0.023	–1.633			17
	13 485.554	3012.186	33 188.811	0.008	0.020	–1.692		–0.09	17
	12 920.933	2961.795	33 753.445	0.077	0.194	–0.712			20
	12 070.491	2889.003	34 603.874	0.010	0.024	–1.620			17
	11 951.660	2879.115	34 722.707	0.033	0.078	–1.107		–0.47	20
	4904.869	2393.362	41 769.497	0.447	0.732	–0.136		–0.07	14
	3644.633	2323.261	43 029.730	0.183	0.282	–0.550		–0.62	19
	3050.863	2291.635	43 623.516	0.020	0.029	–1.531			19
	0.00	2141.828	46 674.387	0.010	0.013	–1.874			18
				0.003					
47904.443	28 546.991	5164.536	19 357.430	0.005	0.054	–1.266			15
$\tau = 2.0ns$	27 285.047	4848.449	20 619.394	0.010	0.105	–0.981			17
$J = 2.5$	21 638.008	3806.060	26 266.431	0.143	0.930	–0.031		0.39	17
	20 134.976	3600.051	27 769.464	0.021	0.124	–0.907			16
	18 897.640	3446.485	29 006.754	0.018	0.097	–1.014			19
	17 830.392	3324.168	30 074.065	0.016	0.081	–1.093			19
	15 084.288	3046.041	32 819.952	0.024	0.101	–0.996		0.04	23[e]
	14 359.454	2980.197	33 545.040	0.006	0.024	–1.620			18
	13 485.554	2904.530	34 418.889	0.030	0.113	–0.947			17

Table 5. continued.

Upper level[a] $(cm)^{-1}$	Lower level $(cm)^{-1}$	λ_{Air} (Å)	σ $(cm)^{-1}$	BF^b	gf	log gf This work	APH[c]	CB[d]	Unc. (% in gf)
	12 920.933	2857.649	34 983.523	0.038	0.141	–0.850		–0.35	18
	12 070.491	2789.827	35 833.945	0.034	0.119	–0.923			18
	6344.381	2405.424	41 560.070	0.433	1.126	0.052		0.21	15
	4904.869	2324.890	42 999.584	0.199	0.485	–0.315		–0.49	18
	3644.633	2258.686	44 259.818	0.011	0.026	–1.590			18
	3050.863	2228.784	44 853.579	0.004	0.009	–2.031			19
				0.008					
49840.585	31 877.888	5565.550	17 962.686	0.002	0.036	–1.448			18
$\tau = 3.1ns$	28 458.225	4675.443	21 382.363	0.008	0.090	–1.048			17
$J = 4.5$	28 104.889	4599.439	21 735.691	0.031	0.313	–0.504			16
	23 145.617	3744.960	26 694.968	0.072	0.487	–0.312		0.40	16
	21 638.008	3544.763	28 202.569	0.007	0.040	–1.402			16
	17 710.827	3111.479	32 129.740	0.002	0.011	–1.976			15
	17 389.109	3080.628	32 451.489	0.264	1.212	0.083		0.37	17
	15 084.288	2876.331	34 756.309	0.217	0.868	–0.062		0.28	17
SA	8361.846	2410.140	41 478.755	0.376	1.057	0.024		0.24	15
	6344.381	2298.343	43 496.218	0.019	0.048	–1.320			19
				0.003					
52340.079	32 778.16	5110.551	19 561.912	0.007	0.124	–0.908			17
$\tau = 1.9ns$	31 877.888	4885.698	20 462.188	0.004	0.063	–1.202			16
$J = 3.5$	28 546.991	4201.718	23 793.086	0.002	0.025	–1.595			15
	28 458.889	4186.095	23 881.883	0.003	0.031	–1.512			17
	28 104.889	4125.069	24 235.180	0.010	0.111	–0.953			18
	21 638.008	3256.162	30 702.151	0.064	0.427	–0.370			20
	17 389.109	2860.310	34 950.978	0.061	0.316	–0.500		0.00	21
	17 368.915	2858.660	34 971.153	0.008	0.043	–1.365			16
	15 084.288	2683.349	37 255.797	0.458	2.082	0.319		0.64	14
	13 485.554	2572.930	38 854.557	0.017	0.070	–1.154			20
	12 070.491	2482.516	40 269.558	0.002	0.009	–2.040			18
	8361.846	2273.149	43 978.248	0.072	0.235	–0.628			21
	6344.381	2173.434	45 995.709	0.013	0.038	–1.419			19
	4904.869	2107.470	47 435.221	0.043	0.122	–0.915			18
	3050.863	2028.188	49 289.231	0.179	0.464	–0.334			18
				0.056					

[a] SA indicates corrected for self absorption.
[b] Last number in each group represents the residual.
[c] Values reported by Andersen et al. (1976).
[d] Values reported by Corliss & Bozman (1962).
[e] Blended line.

Table 6. Finding list for Hf II transitions sorted by wavelength.

$\lambda_{\rm Air}$ (Å)	Lower level (cm)$^{-1}$	Upper level (cm)$^{-1}$	log gf	Unc. (% of gf)
2028.188	3050.863	52 340.079	–0.334	18
2107.470	4904.869	52 340.079	–0.915	18
2141.828	0.00	46 674.354	–1.874	18
2150.073	0.00	46 495.401	–2.568	15
2173.435	6344.381	52 340.079	–1.419	19
2190.218	0.00	45 643.263	–1.345	19
2228.784	3050.863	47 904.443	–2.031	19
2258.686	3644.633	47 904.443	–1.590	18
2273.149	8361.846	52 340.079	–0.628	21
2288.627	0.00	43 680.787	–2.544	44
2291.635	3050.863	46 674.354	–1.531	19
2298.343	6344.381	49 840.585	–1.320	19
2322.476	0.00	43 044.258	–0.140	12
2323.261	3644.633	46 674.354	–0.550	19
2324.890	4904.869	47 904.443	–0.315	18
2332.965	3644.633	46 495.401	–0.946	16
2337.338	0.00	42 770.596	–1.245	21
2351.216	0.00	42 518.148	–0.331	19
2380.305	3644.633	45 643.263	–0.513	14
2393.363	4904.869	46 674.354	–0.136	14
2405.424	6344.381	47 904.443	0.052	15
2410.140	8361.846	49 840.585	0.024	15
2460.495	3050.863	43 680.787	–0.254	15
2482.516	12070.491	52 340.079	–2.040	18
2496.990	3644.633	43 680.787	–0.581	19
2516.883	3050.863	42 770.596	0.039	9
2532.981	3050.863	42 518.148	–2.004	18
2537.333	3644.633	43 044.258	–1.051	24
2571.675	3644.633	42 518.148	–0.071	15
2572.930	13 485.554	52 340.079	–1.154	20
2578.148	4904.869	43 680.787	–0.617	17
2657.844	4904.869	42 518.148	–0.902	21
2677.554	6344.381	43 680.787	–1.866	17
2683.349	15 084.288	52 340.079	0.319	14
2789.827	12 070.491	47 904.443	–0.923	18
2820.225	3050.863	38 498.566	–0.044	13
2857.649	12 920.933	47 904.443	–0.850	18
2858.660	17 368.915	52 340.079	–1.365	16
2860.310	17 389.109	52 340.079	–0.500	21
2861.009	0.00	34 942.411	–0.693	20
2876.332	15 084.288	49 840.585	–0.062	17
2879.115	11 951.660	46 674.354	–1.107	20
2889.003	12 070.491	46 674.354	–1.620	17
2894.037	11 951.660	46 495.401	–1.770	18
2904.531	13 485.554	47 904.443	–0.947	17
2909.917	0.00	34 355.172	–1.645	20
2929.633	0.00	34 123.965	–0.992	14
2961.796	12 920.933	46 674.354	–0.712	20
2967.234	11 951.660	45 643.263	–0.543	17
2975.879	4904.869	38 498.566	–0.299	17
2977.584	12 920.933	46 495.401	–0.911	18
2980.197	14 359.454	47 904.443	–1.620	18
3012.186	13 485.554	46 674.354	–1.692	17
3012.897	0.00	33 180.970	–0.681	14
3046.041	15 084.288	47 904.443	–0.996	23[a]
3080.628	17 389.109	49 840.585	0.083	17
3109.112	6344.381	38 498.566	–0.288	18
3110.877	14 359.454	46 495.401	–0.513	14

Table 6. continued.

$\lambda_{\rm Air}$ (Å)	Lower level (cm)$^{-1}$	Upper level (cm)$^{-1}$	log gf	Unc. (% of gf)
3111.479	17 710.827	49 840.585	–1.976	15
3134.717	3050.863	34 942.411	–0.458	15
3145.305	0.00	31 784.202	–1.624	19
3162.612	12 070.491	43 680.787	–0.774	51[a]
3181.762	15 254.338	46 674.354	–1.633	17
3193.524	3050.863	34 355.172	–0.939	17
3194.191	3644.633	34 942.411	–0.509	17
3195.621	14 359.454	45 643.263	–1.032	18[a]
3199.991	15 254.338	46 495.401	–0.629	15
3215.266	11 951.660	43 044.258	–2.310	22
3217.287	3050.863	34 123.965	–1.519	21
3250.053	12 920.933	43 680.787	–2.397	14
3253.693	3050.863	33 776.300	–0.828	15
3255.273	3644.633	34 355.172	–1.247	20
3256.162	21 638.008	52 340.079	–0.370	20
3279.967	3644.633	34 123.965	–1.221	18
3283.379	12 070.491	42 518.148	–1.448	20
3289.725	15 254.338	45 643.263	–1.611	17
3310.827	13 485.554	43 680.787	–1.270	18
3317.257	8361.846	38 498.566	–2.251	18
3317.984	3050.863	33 180.970	–1.491	20
3318.730	12 920.933	43 044.258	–2.232	23
3324.168	17 830.392	47 904.443	–1.093	19
3328.209	4904.869	34 942.411	–1.519	20
3349.161	12 920.933	42 770.596	–1.623	21
3384.690	3644.633	33 180.970	–1.708	19
3394.576	4904.869	34 355.172	–1.147	18
3399.790	0.00	29 405.129	–0.612	11
3413.734	13 485.554	42 770.596	–1.146	22
3421.437	4904.869	34 123.965	–2.197	20
3443.419	13 485.554	42 518.148	–2.580	17
3446.485	18 897.640	47 904.443	–1.014	19
3462.640	4904.869	33 776.300	–1.699	19
3465.939	17 830.392	46 674.354	–1.778	17
3479.281	3050.863	31 784.202	–1.052	16
3485.170	14 359.454	43 044.258	–1.688	22
3487.576	17 830.392	46 495.401	–0.800	17
3495.743	6344.381	34 942.411	–1.005	18
3495.931	15 084.288	43 680.787	–0.659	17
3518.741	14 359.454	42 770.596	–0.888	20
3535.546	4904.869	33 180.970	–0.689	15
3544.764	21 638.008	49 840.585	–1.402	16
3550.285	14 359.454	42 518.148	–2.358	17
3552.701	3644.633	31 784.202	–1.107	17
3569.034	6344.381	34 355.172	–0.514	12
3594.435	17 830.392	45 643.263	–1.726	18
3597.401	15 254.338	43 044.258	–0.977	22[a]
3599.112	18 897.640	46 674.354	–0.981	18
3600.051	20 134.976	47 904.443	–0.907	16
3622.451	18 897.640	46 495.401	–1.233	17
3633.183	15 254.338	42 770.596	–1.403	21
3644.351	6344.381	33 776.300	–0.657	12
3666.820	15 254.338	42 518.148	–1.766	21
3719.273	4904.869	31 784.202	–0.850	14
3737.869	18 897.640	45 643.263	–0.436	14[a]
3744.960	23 145.617	49 840.585	–0.312	16
3766.916	20 134.976	46 674.354	–0.206	14[a]
3782.780	12 070.491	38 498.566	–1.445	19
3793.373	3050.863	29 405.129	–1.158	25

Table 6. continued.

$\lambda_{\rm Air}$ (Å)	Lower level (cm)$^{-1}$	Upper level (cm)$^{-1}$	log gf	Unc. (% of gf)
3806.061	21 638.008	47 904.443	–0.031	17
3849.511	17 710.827	43 680.787	–0.293	16
3867.316	17 830.392	43 680.787	–0.770	16
3880.814	3644.633	29 405.129	–1.535	27
3933.655	8361.846	33 776.300	–1.813	17
3935.634	17 368.915	42 770.596	–0.911	23
3964.949	17 830.392	43 044.258	–0.988	25
3975.139	17 368.915	42 518.148	–1.697	18
3996.786	13 485.554	38 498.566	–1.555	19
4008.461	17 830.392	42 770.596	–1.233	22
4033.861	18 897.640	43 680.787	–1.314	23[a]
4049.446	17 830.392	42 518.148	–1.112	19
4080.437	4904.869	29 405.129	–1.596	24
4125.069	28 104.889	52 340.079	–0.953	18
4140.199	18 897.640	43 044.258	–2.113	22
4186.095	28 458.889	52 340.079	–1.512	17
4187.663	18 897.640	42 770.596	–1.322	19
4201.718	28 546.991	52 340.079	–1.595	15
4232.387	18 897.640	42 518.148	–0.631	19
4245.845	20 134.976	43 680.787	–1.154	17
4269.695	15 084.288	38 498.566	–1.352	20
4335.154	6344.381	29 405.129	–2.822	22
4370.945	12 070.491	34 942.411	–1.111	17
4416.576	20 134.976	42 770.596	–2.257	18
4466.389	20 134.976	42 518.148	–1.024	19
4486.130	12 070.491	34 355.172	–1.638	18
4508.871	11 951.660	34 123.965	–3.478	17
4533.163	12 070.491	34 123.965	–1.662	19
4535.363	21 638.008	43 680.787	–1.133	15
4539.757	12 920.933	34 942.411	–2.564	17
4599.440	28 104.889	49 840.585	–0.504	16
4605.774	12 070.491	33 776.300	–1.885	20
4659.204	13 485.554	34 942.411	–2.211	16
4664.127	12 920.933	34 355.172	–1.155	16
4675.443	28 458.225	49 840.585	–1.048	17
4714.987	12 920.933	34 123.965	–2.731	18
4731.360	17 368.915	38 498.566	–1.300	19
4735.664	12 070.491	33 180.970	–2.375	16
4809.186	17 710.827	38 498.566	–2.163	15
4843.982	13 485.554	34 123.965	–2.223	18
4848.449	27 285.047	47 904.443	–0.981	17
4857.029	14 359.454	34 942.411	–3.511	14
4885.699	31 877.888	52 340.079	–1.202	16
4926.981	13 485.554	33 776.300	–2.318	19
4934.449	12 920.933	33 180.970	–1.652	19
4999.677	14 359.454	34 355.172	–1.946	20[a]
5034.317	15 084.288	34 942.411	–2.433	15
5040.812	11 951.660	31 784.202	–1.503	20
5058.164	14 359.454	34 123.965	–2.348	19
5071.200	12 070.491	31 784.202	–2.665	40[a]
5075.910	13 485.554	33 180.970	–2.270	17
5080.411	26 996.382	46 674.354	–1.393	16
5110.551	32 778.16	52 340.079	–0.908	17
5126.812	26 996.382	46 495.401	–1.437	58[a]
5156.049	27 285.047	46 674.354	–1.583	16
5164.537	28 546.991	47 904.443	–1.266	15
5187.738	15 084.288	34 355.172	–1.529	20
5204.080	27 285.047	46 495.401	–2.195	12
5298.049	15 254.338	34 123.965	–1.270	21

Table 6. continued.

$\lambda_{\rm Air}$ (Å)	Lower level (cm)$^{-1}$	Upper level (cm)$^{-1}$	log gf	Unc. (% of gf)
5299.832	12 920.933	31 784.202	–2.376	19
5311.594	14 359.454	33 180.970	–1.277	20
5348.391	15 084.288	33 776.300	–2.255	18
5361.350	26 996.382	45 643.263	–1.608	17
5444.046	20 134.976	38 498.566	–1.360	19
5514.988	28 546.991	46 674.354	–1.313	18
5524.343	15 084.288	33 180.970	–1.773	21
5565.551	31 877.888	49 840.585	–1.448	18
5767.199	12 070.491	29 405.129	–2.531	21
5801.681	17 710.827	34 942.411	–2.221	17
5842.220	17 830.392	34 942.411	–1.693	16
6047.994	15 254.338	31 784.202	–2.705	18
6093.122	17 368.915	33 776.300	–2.632	17
6222.810	17 710.820	33 776.300	–2.437	17
6229.630	26 996.382	43 044.258	–1.705	23
6230.834	18 897.640	34 942.411	–1.985	16
6279.845	13 485.554	29 405.129	–2.541	22
6567.393	28 458.225	43 680.787	–1.274	16
6644.593	14 359.454	29 405.129	–1.854	23
6980.901	15 084.288	29 405.129	–1.820	23

[a] Blended line.